

Effect of heat treatment on microstructure of BaTiO₃ solidified by aerodynamic levitator

Chi-hoon Lee^a, Ki-Ju Lee^a, Hyung Giun Kim^b, Sung Hwan Lim^c, M.S. Vijaya Kumar^d, Shinichi Yoda^d and Won-Seung Cho^{a,*}

^aSchool of Materials Science and Engineering, Inha University, 253 Younghyun-Dong, Nam-Gu, Incheon, 402-751, Korea

^bGangwon Regional Division, Korea Institute of Industrial Technology, Gangneung 210-340, Korea

^cDepartment of Advanced Materials Science and Engineering, Kangwon National University, Chuncheon 200-701, Korea

^dInstitute of Space and Astronautical Science, Japan Aerospace Exploration Agency, 3-1-1 Yoshinodai, Chuo-ward, Sagami-hara, Kanagawa, 252-5210, Japan

BaTiO₃ was solidified using an aerodynamic levitator. The effect of heat treatment on microstructure of BaTiO₃ was investigated. Domain walls with a width of ~400 nm were observed in the BaTiO₃ grains. The composition shift from stoichiometric BaTiO₃ to a Ti- or TiO₂-rich composition was attributed to the evaporation of BaO. Ti-rich Ba₆Ti₁₇O₄₀ was formed by a reaction with excess TiO₂ and BaTiO₃ during heat treatment at 1000 °C. A diffuse-interface was observed, indicating that Ba₆Ti₁₇O₄₀ had formed by atomic diffusion.

Key words: Aerodynamic levitation, BaTiO₃, domain, Ba₆Ti₁₇O₄₀, Transmission electron microscopy.

Introduction

Rapidly solidified materials exhibit novel phases and microstructures. The formation of amorphous, metastable phases and dendrite microstructures can be observed. This is well known in metallic systems but can also be observed in ceramic materials, which might result in improved materials properties.

A containerless levitation technique enables a liquid to deeply supercool at a relatively low cooling rate. Materials are solidified under non-equilibrium conditions. The resulting microstructure, composition distribution and properties of materials can be affected significantly [1]. In a previous study on aerodynamic levitation [2], BaTiO₃ was melted using laser beams with a high local energy density and solidified rapidly. The microstructure revealed a unique dendritic network. The use of an aerodynamic levitator is an excellent way of creating novel microstructure in ceramics.

Barium titanate (BaTiO₃) is one of the most important ferroelectric ceramics owing to its outstanding dielectric and ferroelectric properties in applications to multilayer capacitors, thermistors, thermal sensors and electric devices.

Therefore, this study examined the effect of heat treatment on the microstructure of a BaTiO₃ solidified by aerodynamic levitator.

Experimental Procedure

Commercial BaTiO₃ (99.96%, 0.48 μm, tetragonal, Toho Titanium Co., Japan) was used as the starting powder. Rod-type green bodies were sintered at 1200 °C for 1 h in air. Cylindrical pellets, 2.5 mm in diameter, were obtained from the rod. An almost spherical sample was levitated using an aerodynamic levitator with O₂ gas at a flow rate of 660 ml/min. The spherical sample was heated and melted using a CO₂ laser (Firestar-t series, Synrad Inc., USA) with an output power of 100 W. The surface temperature of the levitated droplet was monitored using a pyrometer (Chino IRFBWWHSP, Chino Corp., Japan) at a sampling rate of 100 Hz with a central wavelength of 1.55 mm (InGaAs) and a spot size of 1 mm in diameter. The droplet was cooled by turning off the CO₂ laser.

The levitated BaTiO₃ was heat treated at different temperatures ranging from 600 °C to 1000 °C for 1 h in air. The surface morphologies and cross-sectional microstructures of the samples were analyzed by scanning electron microscopy (SEM: JSM-5500, Jeol).

The levitated samples were crushed and ground using an agate mortar and pestle. The powdered material was used for powder X-ray diffraction (XRD, DMAX-2500, Rigaku, Japan). The crystalline structure and lattice parameters of the samples were analyzed by conventional powder XRD (40 kV, 100 mA) and micro-beam XRD (μXRD, D/Max Rapid-s, Rigaku, Japan). μXRD allows an examination of very small sample areas. The diameter of the analysis area was limited to approximately 800 μm by the collimator.

*Corresponding author:
Tel : +82-32-860-7528
Fax: +82-32-862-5546
E-mail: wscho@inha.ac.kr

The experimental conditions of μ XRD were as follows: Cu $K\alpha$ ($\lambda = 1.5406\text{\AA}$) radiation (40 kV, 30 mA); measuring range, 20° - 80° ; omega (ω), 20° - 40° ; phi (ϕ), -45° - 45° ; step, 0.044° ; and exposure time, 10 min. The lattice parameters of the phases were calculated using the Nelson-Riley extrapolation [3], which allows a precise determination of the lattice constant.

Transmission electron microscopy (TEM) was used to characterize the microstructure after heat-treatment. The study samples were prepared as thin foils using the focused ion beam (FIB-SEM) method. The method of sample preparation was based on the ion bombardment for thinning a part of the slab in a scanning electron microscope dual beam (SEM-FIB Nova 200).

The specimens were coated with Pt to prevent surface damage from Ga^+ ion milling during TEM sample preparation. The specimens were then characterized by field-emission TEM (JEM-2100F, 200 kV). Atomic modeling was carried out to understand the atomic structure using Crystal Kit software [4].

Results and Discussion

Fig. 1 shows the temperature-time profile of BaTiO_3 ($T_m = 1620^\circ\text{C}$). BaTiO_3 was superheated above its melting point and held at that temperature for 30 secs to obtain a homogeneous melt.

Recalescence was observed at $\sim 976^\circ\text{C}$, indicating that the undercooled melt had solidified into a polycrystalline BaTiO_3 phase. The degree of recalescence was found to be $\sim 644^\circ\text{C}$. The measured recalescence time interval (t_R) and plateau time (t_P) were ~ 20 ms and ~ 100 ms, respectively.

Fig. 2 shows SEM images of the levitated BaTiO_3 sample. Nucleation started from the nucleation point, and propagated in the radial direction throughout the entire sample. Figs. 2(c) and (d) show a cross section of the levitated sample. The sample was polished carefully until the cross section met the nucleation point, and thermally etched at 1400°C in air without a

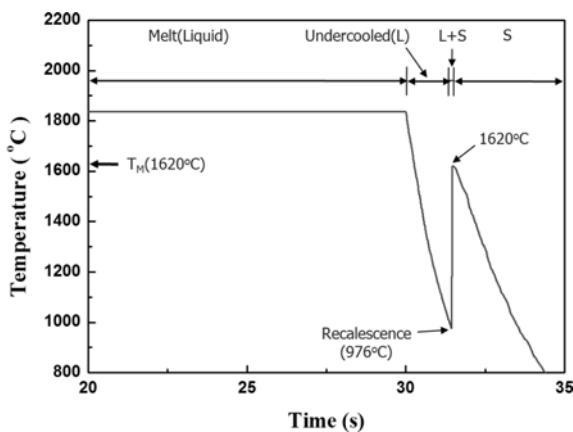


Fig. 1. Temperature-time profile for BaTiO_3 during aerodynamic levitation. L and S denote the solid and liquid, respectively.

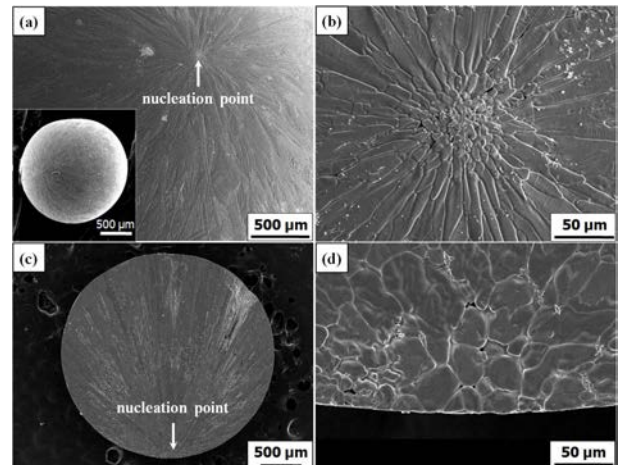


Fig. 2. SEM images of (a) surface of as-levitated BaTiO_3 sample and (b) nucleation point at surface, (c) polished cross-section and (d) nucleation point at internal cross-section.

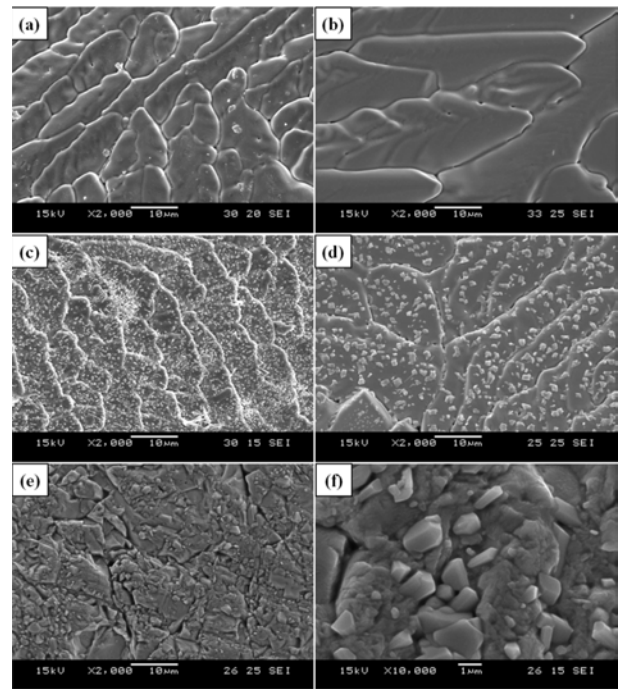


Fig. 3. SEM images of the surface (a-d) and cross-section (e, f) of BaTiO_3 . The levitated samples were heat-treated at different temperatures and times; (a) as-levitated, (b) 600°C -1 h, (c) 1000°C -1 h, and (d) 1000°C -12 h (surface). (e) 1000°C -12 h (cross-section), and (f) magnified image of (e).

holding time. The nucleation point consisted of many equiaxed grains. In addition, an equiaxed-to-cellular dendrite transition was observed at the region apart from the nucleation point.

Fig. 3 shows SEM images of the surface of the levitated BaTiO_3 sample. The levitated samples were heat treated at different temperatures and times. No change in surface morphology was observed until 600°C . On the other hand, many crystals nucleated after heat-treatment at 1000°C for 1h. Crystal growth during prolonged heat treatment (1000°C for 12 hrs)

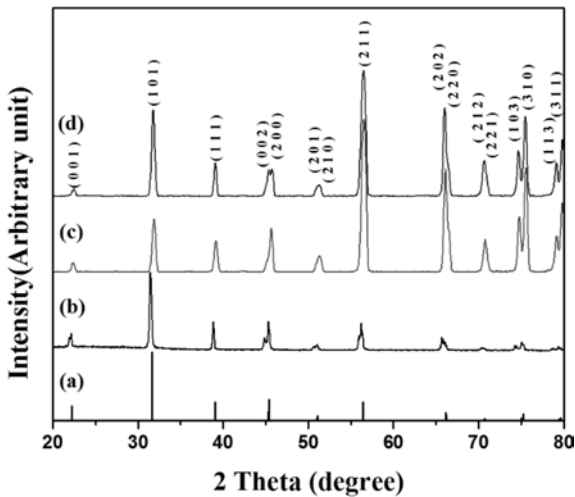


Fig. 4. XRD patterns of the BaTiO₃ samples; (a) standard diffraction patterns corresponding to tetragonal BaTiO₃ (JCPDS, card No.75-2122), (b) Powder XRD patterns of the as-levitated sample, μ XRD patterns of (c) as-levitated and (d) heat-treated BaTiO₃ samples (1000 °C for 1 h, air).

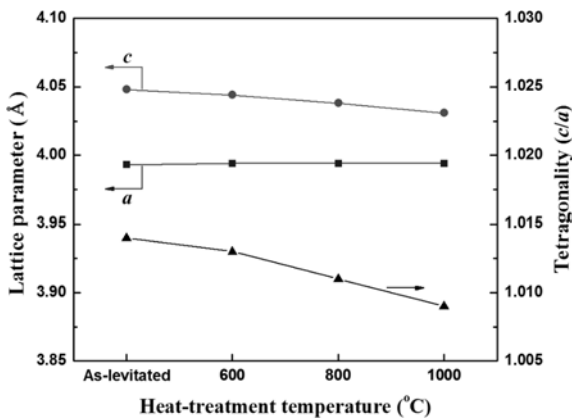


Fig. 5. Lattice parameters (a, c) and tetragonality (c/a) of the BaTiO₃ sample as a function of the heat-treatment temperature. The lattice parameters were measured for the powder after crashing the levitated samples for conventional powder XRD analysis.

occurred by coalescence, as shown in Fig. 3(d). The shape of the crystals was rectangular, rather than spherical.

In a previous study [2], mass loss due to evaporation can occur during laser heating in the superheating stage. Hence, there might be a difference in the composition of the levitated droplet between the

periphery and center region. To examine the effect of a composition difference on the formation of new crystals, cross sections of levitated samples were also heat treated at 1000 °C for 1 hr and 12 hrs. New crystals were formed, even in the interior region, indicating they had formed simultaneously, regardless of the location of the sample.

Fig. 4 shows XRD patterns of the levitated and heat-treated BaTiO₃ samples. The standard diffraction patterns corresponded to tetragonal BaTiO₃ (JCPDS, card No.75-2122). Conventional XRD was conducted on the powdered sample. μ XRD was conducted on the as-levitated and heat-treated sample (1000 °C for 1h, air). The split between the two peaks corresponding to the (103) and (310) planes at approximately 75 °, indicates that all the BaTiO₃ samples had a tetragonal crystalline structure. The μ XRD patterns shifted toward a higher diffraction angle compared to the standard diffraction patterns. This shift in peak position may be due to compressive residual stress developed on the surface of the droplet during rapid solidification. Hossain *et al.* [5] examined the residual stresses in quenched stainless-steel spheres, and reported that compressive residual stress occurred along the cooling surface.

Fig. 5 shows the lattice parameters and tetragonality of the BaTiO₃ sample as a function of the heat-treatment temperature. The lattice parameters were calculated for the powdered samples from the conventional powder XRD patterns. No substantial difference in the lattice parameter, a, was observed but the lattice parameter, c, decreased with increasing heat-treatment temperature. As a result, the tetragonality of the tetragonal phase decreased with increasing heat-treatment temperature. This shows that the crystallization kinetics of the tetragonal phase in BaTiO₃ is affected by the heat-treatment temperature. The lattice parameter and tetragonality was also measured from the μ XRD patterns. Table 1 lists the lattice parameters of the as-levitated and heat-treated BaTiO₃ samples. The lattice parameters measured from two types of XRD instruments showed little differences in the absolute values.

Fig. 6 shows the TEM bright-field images of the domain walls and diffraction pattern of the as-levitated BaTiO₃ sample. The grain size of the levitated BaTiO₃ was more than 10 μ m. The grains consisted of domains

Table 1. Lattice parameters and tetragonality of the as-levitated and heat-treated BaTiO₃ samples. XRD analysis was conducted using two types of XRD.

Type of XRD	Specimen	Structure	a (Å)	c (Å)	Tetragonality	Volume (nm ³)
Conventional Powder XRD	as-levitated	tetragonal	3.993	4.048	1.014	0.0645
	heat-treated (1000 °C-1 h)	tetragonal	3.994	4.031	1.009	0.0643
Micro-beam XRD	as-levitated	tetragonal	3.976	4.052	1.019	0.0641
	heat-treated (1000 °C-1 h)	tetragonal	3.982	4.011	1.007	0.0636

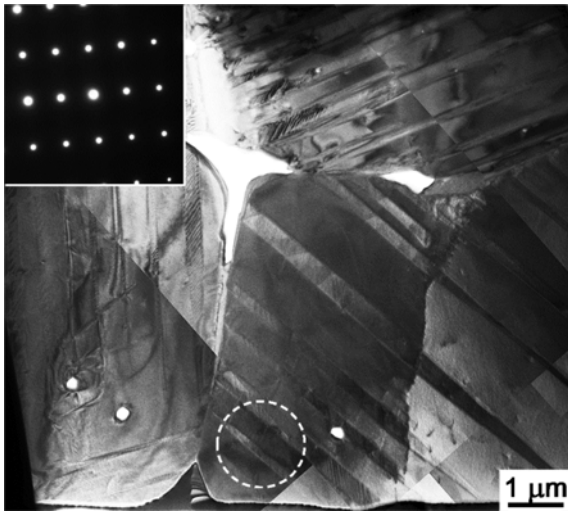
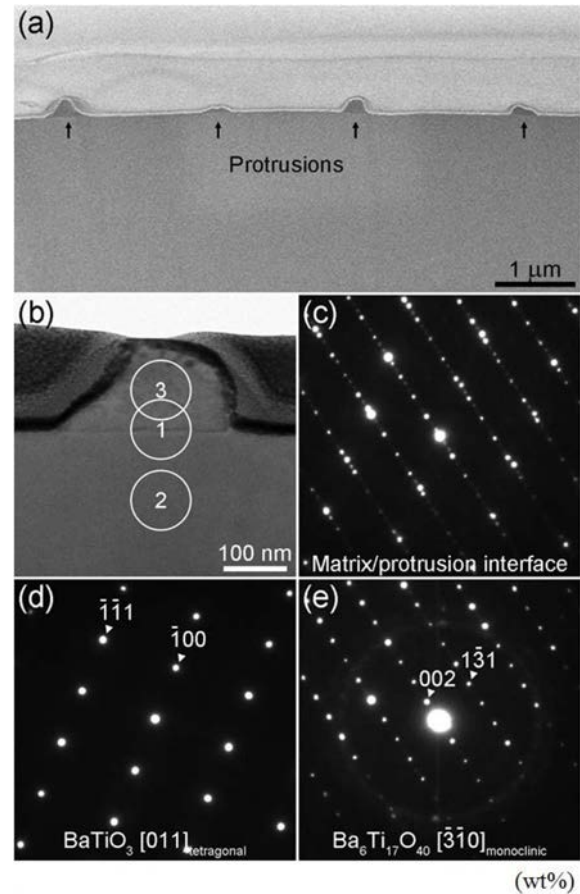


Fig. 6. TEM bright-field image of the domain-walls and diffraction pattern in the as-levitated BaTiO₃ sample. Selected area diffraction pattern obtained from the domain indicated by the dotted white circle.

in which the polar axes (tetragonal axis) of all the tetragonal unit cells were in the same direction. Domains in tetragonal ferroelectric ceramics are generated to minimize the internal stress developed during the transformation from cubic to tetragonal at the Curie temperature [6]. Domain walls with an almost constant width (~400 nm) were observed. This is consistent with that reported by Arlt *et al.* [7], who showed that the domain-wall width is practically constant for a grain size > 10 μm. Hoshina *et al.* [8] reported that the increase in permittivity with decreasing grain size was due to the domain size effect, and suggested that it is possible to control the measured permittivity of BaTiO₃ ceramics by controlling the domain configuration. The measured permittivity of the levitated BaTiO₃ sample was ~4,000 [2]. Hoshina *et al.* reported that the permittivity of BaTiO₃ with domain walls of 400 nm corresponded to ~3,700, showing relatively good agreement with the result of the present study.

Fig. 7 shows SEM and TEM images along with results of energy dispersive spectrometry (EDS) analysis of the protrusion formed on the surface of the heat-treated BaTiO₃ sample (1000 °C for 1 h) after levitation. Fig. 7(a) gives a cross-sectional view of new crystals. Fig. 7(b) shows a TEM bright-field image of a protrusion; Fig. 7(c)-(e) presents the diffraction patterns taken from the matrix/protrusion interface (“①”, see Fig. 7(b)), the matrix (“②”) and protrusion (“③”), respectively. The diffraction patterns were recorded by tilting the foil to an exact zone-axis. These diffraction patterns were identified as tetragonal BaTiO₃ (t-BT, zone-axis: [011]_{t-BT}) and monoclinic Ba₆Ti₁₇O₄₀ (m-BTO, zone-axis: [310]_{m-BTO}). The monoclinic crystal structure of Ba₆Ti₁₇O₄₀ accounts well for the rectangular shaped crystals, as shown in Fig. 3.



Region	Ba	Ti	O
Matrix (②)	69.9	11.3	18.8
Protrusion (③)	50.6	21.7	27.7

Fig. 7. SEM and TEM images, diffraction patterns, and EDS analysis of new crystal (protrusion) formed on the surface of the heat-treated BaTiO₃ sample after levitation; (a) Cross-sectional SEM image, (b) TEM bright-field image, (c) diffraction pattern at the interface (①, see image (b)), (d) diffraction pattern at matrix (②), and (e) diffraction pattern at protrusion (③). The EDS analysis results for the matrix and protrusion are indicated below.

The electron diffraction patterns taken from the region of the grain with the protrusion indicated the orientation relationships between BaTiO₃ and Ba₆Ti₁₇O₄₀ to be (111)_{t-BT}//(002)_{m-BTO} and [011]_{t-BT}//[310]_{m-BTO}. Therefore, the close-packed planes of Ba₆Ti₁₇O₄₀ lie parallel to the close-packed planes of BaTiO₃. Earlier studies reported the orientation relationship between t-BT and m-BTO [9-12]. Kraševac *et al.* [9] reported that the orientation relationships were (111)_{t-BT}//(001)_{m-BTO}, (001)_{t-BT}//(101)_{m-BTO}, and [110]_{t-BT}//[010]_{m-BTO}. The EDS showed that the Ba₆Ti₁₇O₄₀ were Ti- and O-rich compared to the BaTiO₃ matrix.

Fig. 8 presents a high-resolution TEM (HRTEM) image (a), digital diffractograms (b, c), and atomic models (d, e) at the BaTiO₃/Ba₆Ti₁₇O₄₀ interface. The inset in Fig.

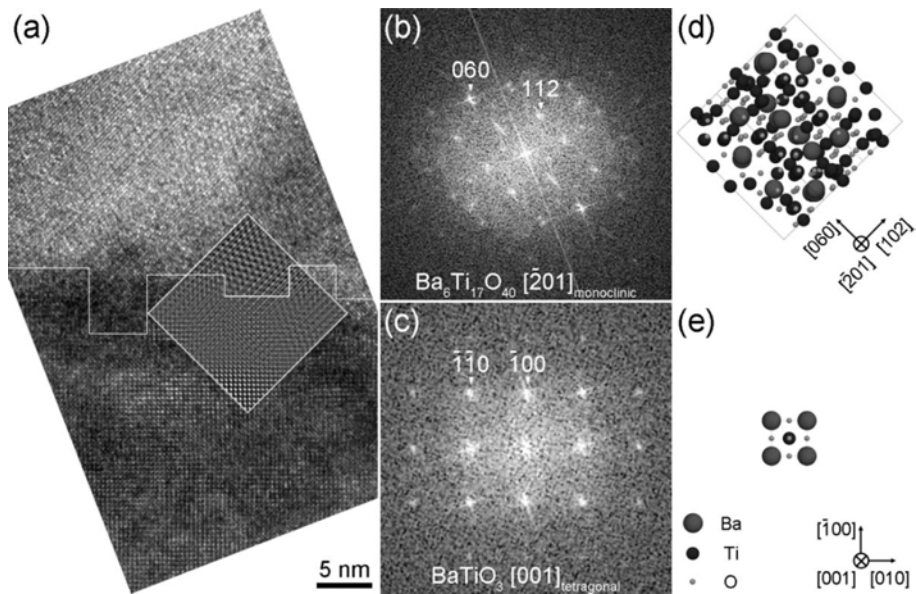


Fig. 8. High-resolution TEM (HRTEM) image, diffraction patterns and atomic models at the interface of BaTiO₃/Ba₆Ti₁₇O₄₀; (a) HRTEM image with the inset, showing inverse Fourier transformation at the protrusion (top)/matrix (bottom) interface, (b) digital diffractogram of protrusion, (c) digital diffractogram of matrix region, (d) atomic model of Ba₆Ti₁₇O₄₀ unit-cell, and (e) atomic model of BaTiO₃ unit-cell.

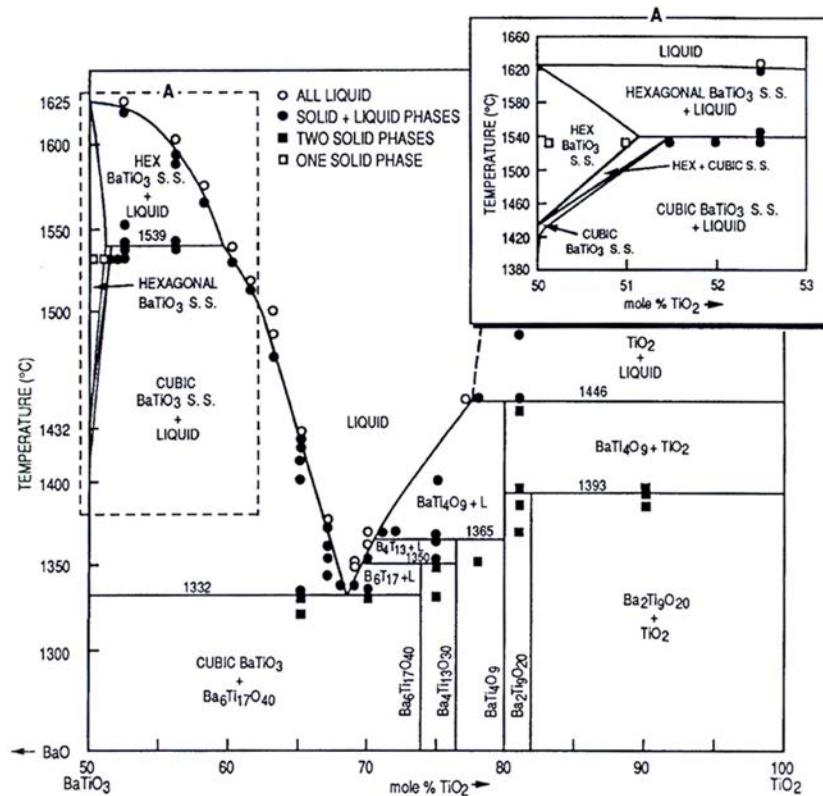


Fig. 9. BaTiO₃-TiO₂ equilibrium phase diagram [21].

8(a) shows an inverse Fourier transformation at the interface of the protrusion (m-BTO: along [201]_{m-BTO}) and matrix (t-BTO: along [001]_{t-BT}). A diffuse-interface was observed, as indicated by the non-faceted white line [13], indicating that the protrusion was formed on the surface by atomic diffusion.

Based on HRTEM analysis, the protrusion was

identified as a Ti-rich Ba₆Ti₁₇O₄₀ phase. Therefore, the cause for the formation of Ba₆Ti₁₇O₄₀ will be discussed. By laser heating in the superheating stage, BaTiO₃ will be decomposed to BaO, TiO and TiO₂. This presumption is reasonable because BaTiO₃ decomposes to BaO, TiO and TiO₂ by electron beam melting, as reported by Feuersanger *et al.* [14].

The mass loss rate due to evaporation in the superheating stage depends on the vapor pressure of BaO, TiO and TiO₂. The vapor pressures (p, mmHg) of BaO, TiO and TiO₂ were determined using the following equations obtained from the literature [15, 16]:

$$\log p(\text{BaO}) = \frac{-21900}{T} + 9.990, (1200-1700 \text{ K})$$

$$\log p(\text{TiO}) = \frac{-25450}{T} + 9.008, (2300-2500 \text{ K})$$

$$\log p(\text{TiO}_2) = \frac{-25120}{T} + 8.681, (2300-2500 \text{ K})$$

where T is the temperature in Kelvin. The BaO vapor pressure at temperature (≥ 1893 K) above the melting point of BaTiO₃ could not be estimated due to the upper temperature limit. The calculated vapor pressures at the upper (1700 K for BaO) and lower temperature limit (at 2300 K for TiO and TiO₂) were 1.28×10^{-3} (for BaO), 8.77×10^{-3} (for TiO), and 5.74×10^{-3} (for TiO₂) mmHg. These values are in the same order of 10^{-3} despite the large temperature difference of 600 K. The exponential temperature dependence of the vapor pressure suggests that the vapor pressure of BaO at high temperatures (≥ 1893 K) is much higher than those of TiO, and TiO₂. A composition shift from stoichiometric BaTiO₃ to a Ti- or TiO₂-rich composition is expected because of the anticipated loss of BaO due to the high vapor pressure. Sharama *et al.* [17] reported that the solubility of TiO₂ in BaTiO₃ is < 0.1 mol%, indicating that TiO₂ is practically insoluble in BaTiO₃. Upon cooling from temperatures above the melting point, excess TiO₂ will be incorporated into the growing BaTiO₃ solid. The excess TiO₂ reacts with the BaTiO₃, forming a Ba₆Ti₁₇O₄₀ phase [12]:



This result is consistent with earlier studies [11, 12, 18-20]. Excess Ti or TiO₂ in BaTiO₃ was reported to form Ba₆Ti₁₇O₄₀ by a certain topotaxial reaction involving Ba outdiffusion and Ti and O indiffusion.

Fig. 9 shows a high-temperature phase diagram [21] for the system BaTiO₃-TiO₂. As observed from the phase diagram, the formation of Ti-rich barium titanates depends on the Ba to Ti ratio and temperature. Stable Ba₆Ti₁₇O₄₀ exists at a Ti-rich composition adjacent to the stoichiometric BaTiO₃ composition. Therefore, Ba₆Ti₁₇O₄₀ was formed by a reaction with excess TiO₂ and BaTiO₃ during heat treatment. The crystallization kinetics of Ba₆Ti₁₇O₄₀ are believed to be controlled by a diffusion process.

Conclusions

BaTiO₃ was solidified using an aerodynamic levitator. The effect of heat treatment on microstructure of BaTiO₃

was examined by SEM and TEM. Domain walls, ~ 400 nm in width, were observed in the BaTiO₃ grains. The composition shift from a stoichiometric BaTiO₃ to Ti- or TiO₂-rich composition occurred due to the evaporation of BaO. Ti-rich Ba₆Ti₁₇O₄₀ was formed by a reaction with excess TiO₂ and BaTiO₃ during heat treatment at 1000 °C. A diffuse-interface was observed, indicating that Ba₆Ti₁₇O₄₀ was formed by atomic diffusion.

Acknowledgement

This study was supported by the NSL (National Space Lab) program through the National Research Foundation of Korea funded by the Ministry of Education, Science and Technology (NRF-2011-0030870).

References

1. J. Yu, N. Koshikawa, Y. Arai, S. Yoda, and H. Saitou, J. Cryst. Growth 231 (2001) 568-576.
2. K.J. Lee, C.H. Lee, G.W. Lee, W.S. Hwang, C.H. Lee, S. Yoda, and W.S. Cho, Thermochim. Acta 542 (2012) 37-41.
3. J.B. Nelson and D.P. Riley, Proc. Phys. Soc. 57 (1945) 160-177.
4. <http://www.totalresolution.com/CrystalKitX.html>
5. S. Hossain, M.R. Daymond, C.E. Truman, and D.J. Smith, Mat. Sci. Eng. A 373 (2004) 339-349.
6. G. Arlt, J. Mat. Sci. 25 (1990) 2655-2666.
7. G. Arlt, D. Hennings, and G. de With, J. Appl. Phys. 58 (1985) 1619-1625.
8. T. Hoshina, K. Takizawa, J. Li, T. Kasama, H. Kakemoto, and T. Tsurumi, Jpn. J. Appl. Phys. 47 [9] (2008) 7607-7611.
9. V. Kraševic, M. Drogenik, and D. Kolar, J. Am. Ceram. Soc. 70 [8] (1987) 193-195.
10. S.J. Zheng, K. Du, X.H. Sang, and X.L. Ma, Philos. Mag. 87 [34] (2007) 5447-5459.
11. A. Lotnyk, A. Graff, S. Senz, N.D. Zakharov, and D. Hesse, Solid State Sci. 10 (2008) 702-708.
12. S. Senz, A. Graff, W. Blum, D. Hesse, J. Am. Ceram. Soc. 81[5] (1998) 1317-1321.
13. D.A. Potter and K.E. Easterling, in "Phase Transformation in Metals and Alloys-2nd edition" (Chapman & Hall, 1992) p. 169.
14. A.E. Feuersanger, A.K. Hagenlocher, and A.L. Solomon, J. Electrochem. Soc. 111 [12] (1964) 1387-1391.
15. E.A. Brandes and G.B. Brook, in "Smithells Metals Reference Book-7th edition" (Butterworth-Heinemann Ltd, Oxford, 1992) p. 8-54.
16. G.A. Semenov and S.I. Lopatin, Russ. J. App. Chem. 74 [6] (2001) 901-906.
17. R. K. Sharma, N. H. Chan, and D. M. Smyth, J. Am. Ceram. Soc. 64 [8] (1981) 448-451.
18. D. Völtzke, S. Gablenz, H.P. Abicht, R. Schneider, E. Pippel, and J. Woltersdorf, Mater. Chem. Phys. 61 (1999) 110-116.
19. D. Hesse, A. Graff, S. Senz, and N.D. Zakharov, Mater. Sci. Forum 294-296 (1999) 597-600.
20. X. Xu and G.E. Hilmas, J. Am. Ceram. Soc. 89[8] (2006) 2496-2501.
21. K.W. Kirby and B.A. Wechsler, J. Am. Ceram. Soc. 74 [8] (1991) 1841-1847.